Macromolecular Research, Vol. 16, No. 1, pp 15-20 (2008)

Tumoral Accumulation of Long-Circulating, Self-Assembled Nanoparticles and Its Visualization by Gamma Scintigraphy

Yong Woo Cho

Department of Chemical Engineering, Hanyang University, Ansan 426-791, Korea

Yoo-Shin Kim, In-San Kim, and Rang-Woon Park*

Advanced Medical Technology Cluster for Diagnosis and Prediction, Department of Biochemistry and Cell Biology, School of Medicine, Kyungpook National University, Daegu 700-422, Korea

Seung Jun Oh, Dae Hyuk Moon, and Sang Yoon Kim

Asan Medical Center, University of Ulsan College of Medicine, Seoul 138-736, Korea

Ick Chan Kwon

Biomedical Research Center, Korea Institute of Science and Technology, Seoul 136-791, Korea

Received May 9, 2007; Revised September 11, 2007

Abstract: The enhanced permeability and retention (EPR) effect is used extensively for the passive targeting of many macromolecular drugs for tumors. Indeed, the EPR concept has been a gold standard in polymeric anticancer drug delivery systems. This study investigated the tumoral distribution of self-assembled nanoparticles based on the EPR effect using fluorescein and radio-labeled nanoparticles. Self-assembled nanoparticles were prepared from amphiphilic chitosan derivatives, and their tissue distribution was examined in tumor-bearing mice. The size of the nanoparticles was controlled to be 330 nm, which is a size suited for opening between thedefective endothelial cells in tumors. The long-circulating polymer nanoparticles were allowed to gradually accumulate in the tumors for 11 days. The amount of nanoparticles accumulated in the tumors was remarkably augmented from 3.4%ID/g tissue at 1 day to 25.9%ID/g tissue at 11 days after i.v. administration. The self-assembled nanoparticles were sustained at a high level throughout the 14 day experimental period, indicating their long systemic retention in the blood circulation. The γ-images provided clear evidence of selective tumor localization of the ^{131}I-labeled nanoparticles. Confocal microscopy revealed the fluorescein-labeled nanoparticles to be preferentially localized in the perivascular regions, suggesting their extravasation to the tumors through the hyperpermeable angiogenic tumor vasculature. This highly selective tumoral accumulation of nanoparticles was attributed to the leakiness of the blood vessels in the tumors and their long residence time in the blood circulation.

Keywords: nanoparticles, EPR effect, tumor targeting, long-circulating, gamma scintigraphy.

Introduction

Since Maeda's landmark work[1] in 1986 suggested the concept of 'the enhanced permeability and retention (EPR)' effect, the hyperpermeable angiogenic tumor vasculature has been an excellent target for polymeric anticancer drug delivery systems. A number of polymer-drug conjugates and nanoparticles based on the EPR effect have been developed and some are being tested clinically and awaiting market approval. Typical polymer-drug conjugates include: styrene maleic anhydride (SMA)-neocarzinostatin (NCS) called SMANCS[1-3], *N*-(2-hydroxypropyl) methacrylamide (HPMA) copolymer-drug conjugates,[4-6] and poly(glutamate)-drug conjugates.[7] The covalent attachment of an anticancer drug to a macromolecule changes its pharmacokinetics *in vivo*. The EPR effect has been shown to be effective with macromolecules having a molecular weight larger than 40 kDa.[2] In general, most macromolecular prodrugs preferentially accumulated in tumor tissues.[1-3,8] Numerous polymer-based nanoparticles have also been studied for delivery of therapeutic agents and imaging probes; these have yielded promising results.[9-16]

Conventional low molecular weight drugs have plasma half-lives of a few minutes, but their half-lives extend up to

*Corresponding Author. E-mail: nwpark@knu.ac.kr

a few hours in macromolecular prodrugs.[3] In order to rationally design polymeric drug delivery systems based on passive tumor targeting by the EPR effect, the size of the drug delivery system traversing the open vascular gaps must first be optimized. Most tumor vessels are unusually leaky. The tumors grown subcutaneously in dorsal chambers of mice have openings between defective endothelial cells ranging in size from 100 to 1,000 nm and the majority of the gaps have been shown to be between 200 and 900 nm.[17-21] Considering that the hydrodynamic diameters of most polymer-drug conjugates in aqueous solutions do not exceed 20 nm and that normal tissues with a discontinuous endothelium such as the liver, spleen, and bone marrow have endothelial gaps of around 100 nm, water-soluble polymer-drug conjugates might not fully realize selective targeting based on the hyperpermeable angiogenic tumor vasculature.

In this study, to actualize passive tumor targeting by the EPR effect, we prepared self-assembled nanoparticles exhibiting long stability in blood circulation from amphiphilic chitosan derivatives. The size of nanoparticles was controlled to a mean diameter of 330 nm, which is larger than endothelial gaps in normal tissues but smaller than characteristic pore cut-off sizes in tumors. Fluorescein isothiocyanate (FITC)-labeled or ^{131}I-labeled nanoparticles were injected into the tail veins of tumor-bearing mice to demonstrate their selective tumoral distribution and long stability in blood circulation.

Experimental

Materials. Glycol chitosan (GC, molecular weight of 250 kDa, degree of deacetylation 88%) and FITC were purchased from Sigma (St. Louis, MO, USA). GC was purified by dialysis against water, followed by lyophilization. Cell culture media, fetal bovine serum (FBS) and trypsin-EDTA were purchased from Gibco-BRL (Grand Island, NY, USA). All other chemicals were of analytical grade and used as received.

Preparation of Self-Assembled Nanoparticles. FITC-glycol chitosan (FGC) nanoparticles were prepared in a manner similar to the procedure described in previous reports.[16,22,23] The size of the FGC nanoparticles was controlled to a mean diameter of 330 nm by an emulsion/solvent evaporation method.[22] Briefly, FGCs were suspended in a phosphate-buffered saline solution (PBS, pH 7.4) at different concentrations under gentle shaking and chloroform was slowly added to the nanoparticle suspensions. Each suspension was then sonicated five times using a probe-type sonicator (Sigma Ultrasonic Processor, GEX-600, St. Louis, MO, USA) at 90 W for 2 min each, in which the pulse was turned off for 1 s in 5 s intervals. The nanoparticle suspensions were then passed through a syringe filter (pore size 0.45 μm, Millipore, Billerica, MA, USA) and stored at room temperature.

Characterization of Self-Assembled Nanoparticles. The particle size distribution of nanoparticles was measured by dynamic light scattering using a helium ion laser system (Spectra Physics Laser Model 127-35, Mountain view, CA, USA) tuned to a wavelength of 633 nm. Scattered light was measured at an angle of 90° and was collected with a Brookhaven BI-9000AT autocorrelator (Holtsville, NY, USA). The hydrodynamic diameters of nanoparticles were calculated by the Stokes-Einstein equation.

Body Distribution of Self-Assembled Nanoparticles. B16F10 mouse melanoma cells (ATCC, Rockville, MD, USA) were cultured in RPMI 1640 medium supplemented with 10% FBS at 37 °C in a humidified 5% CO_2 incubator. A suspension of 1×10^6 cells in a physiological saline was inoculated in the subcutaneous dorsa of C57BL/6J mice (7 weeks old, 20-25 g). On the 7th day after subcutaneous inoculation, FGC nanoparticle suspensions (200 μL) were injected into the tail veins of the tumor-bearing mice at a dose of 1.8 mg/kg. After a definite time period of 14 days post-injection, the mice were sacrificed under isofluoran inhalation anesthesia for the collection of blood. Various tissues were then excised, including the heart, kidney, liver, lungs, spleen, and tumor (n = 6 mice for each study group). The quantitative amount of nanoparticles distributed in blood and tissues as expressed as a percentage of the injected dose per gram of tissue (%ID/g tissue) was estimated by a fluorescence measurement, as described previously.[16]

Radioisotope Labeling and Gamma Scintigraphy. For ^{131}I-labeling, *N*-acetyl tyrosine was attached to FGC nanoparticles.[23] GC (475 mg) and *N*-acetyl tyrosine (25.0 mg, 0.11 mmol) were dissolved in distilled water (100 mL). *N*-(3-dimethyl aminopropyl)-*N'*-ethylcarbodiimide hydrochloride (EDC, 63.2 mg, 0.33 mmol) and *N*-hydroxysuccinimide (NHS, 38.0 mg, 0.33 mmol) were added to the aqueous solution containing GC and *N*-acetyl tyrosine. The reaction mixture was stirred overnight, dialyzed against distilled water using a cellulose membrane (MWCO 12000, Spectrum Laboratories, Rancho Dominguez, CA, USA) for 2 days and then freeze-dried. The amount of conjugated *N*-acetyl tyrosine was 4.8 per 100 glucosamine units of GC.

FGC nanoparticles were iodinated with Na^{131}I (Korea Atomic Energy Research Institute, Daejeon, Korea). *N*-Acetyl tyrosine-conjugated FGC nanoparticles (60 mg) were dissolved in 0.5 mL of purified water in a glass test tube, to which six Iodogen beads (Pierce Chemical, Rockford, IL, USA) and 185 MBq (5 mCi)/0.5 mL of Na^{131}I were added. The labeling efficiency was measured by thin layer chromatography on a silica gel plate. A mixture of acetone and ethyl acetate/ethanol (1:1 volume) was used as a solvent. The chromatogram was obtained with a radioactive chromatogram scanner (RadioTLC, AR-2000, Bioscan, Washington DC, USA).

The murine squamous cell carcinoma cell line (SCC7) was cultured in RPMI 1640 medium (Invitrogen Corporation, Bethesda, MD, USA) containing 10% fetal calf serum, 2 mmol/L glutamine and a mixture of 50 IU/mL penicillin and 50 μg/mL streptomycin (BioSource International; Rockville, Md) at 37 °C with 5% CO_2. For scintigraphic imaging

studies, a suspension of 1×10^6 SCC7 cells in physiological saline was injected subcutaneously into 7 week-old male C3H mice. The tumor volume was determined by direct measurement with calipers and calculated using the following formula: $\pi abc/6$, where a is the long diameter, b the short diameter, and c the height. Two weeks after inoculation, 3 mice were injected with 7.4 MBq / 0.2 mL of ^{131}I-labeled nanoparticles (mean diameter of 330 nm) through the tail veins of the tumor-bearing mice. Serial ventral whole-body images were acquired for 10 min at 30 min, 1 h, 2, 4, and 6 days post-injection using a planar γ-camera (Biad, Trionix, Twinsberg, OH, USA) equipped with medium energy collimators.

Confocal Microscopy. Tumor blood vessels were visualized by Hoechst 33342 diffusion.[24-26] Tumor-bearing mice received an intravenous injection of 100 mL of FGC nanoparticles (20 mg/mL) in physiological saline followed 3 days later by 100 mL of 0.2% Hoechst 33342 dye (Molecular Probes, Eugene, OR, USA) in physiological saline immediately prior to sacrifice. The tumors were dissected, embedded in OCT medium (Miles Inc, Elkhart, IN, USA), and then frozen in isopentane in a dry-ice bath. Sections (10 mm) were cut using a cryostat, thawed, and mounted onto slides. The fluorescence was observed in two channels: green (expressing FGC nanoparticles; excitation 490 nm, emission 520 nm) and blue (blood vessels stained with Hoechst 33342; excitation 350 nm, emission 461 nm). The images were acquired using a confocal microscope (TCS SP2, LEICA Microsystems, Nussloch, Germany).

Results

Characterization of Self-Assembled Nanoparticles. All FGCs were prepared by methods similar to those previously reported by our group.[16,22] The FITC content was 2.5 wt%. As previously mentioned, FGC nanoparticles with a mean diameter of 330 nm were prepared by the addition of chloroform to FGC suspensions in water. The size of the nanoparticles and their distribution in aqueous media were measured by dynamic light scattering, as shown in Figure 1.

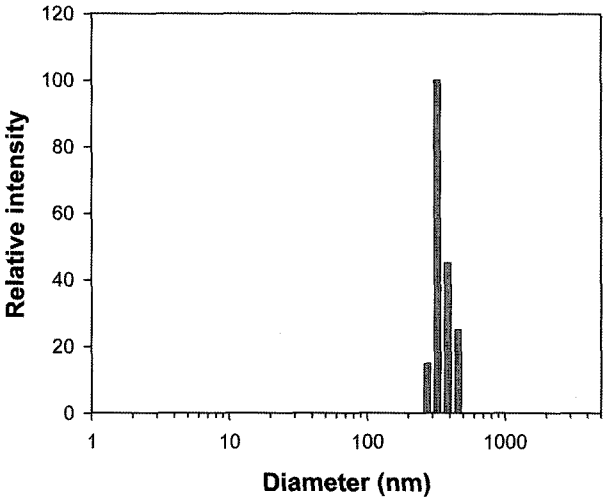

Figure 1. Size distribution of FGC nanoparticles (mean diameter: 330 nm) measured by dynamic light scattering in PBS at a concentration of 1 mg/mL.

Body Distribution of Self-Assembled Nanoparticles. Tissue distribution of the FGC nanoparticles in tumor-bearing mice is shown in Figure 2, as expressed as a percentage of the injected dose per gram of tissue (%ID/g tissue). It is of great significance to note that the tumoral accumulation of FGC nanoparticles gradually augmented for 11 days after i.v. administration. Accumulation in tumors of the nanoparticles increased remarkably from 3.4 %ID/g tissue at 1 day to 25. 9%ID/g tissue at 11 days. One day after i.v. administration, the majority of nanoparticles were distributed in the liver, kidney, blood, urine, and tumor. Three days after of administration, the fluorescence intensities decreased in the blood and urine, but those in other tissues, including the tumor, increased. Among them, the tumoral accumulation was predominantly enhanced. Even 5, 8, and 11 days after injection, the tumoral accumulation was still significantly augmented while accumulation in other tissues decreased. Eleven days after injection, the concentrations of nanoparticles accumulated in tumors were over 3-fold higher than those in other tissues. The amounts of nanoparticles in blood circulation decreased gradually over time but were still at a high level even 14 days after injection (2% of injected dose per milliliter of blood).

Gamma Scintigrahpy. *In vitro* stability of ^{131}I-labeled nanoparticles after incubation in 10% human plasma was > 95% (n = 5) within 1 day. But we found 5.0 ± 2.7% and 10.0 ± 3.4% of unknown ^{131}I-labeled impurities (R_f = 0.7-0.8) at 2 and 3 days after incubation, respectively.

Figure 3 shows the scintigraphic images of mice after tail-vein injection of ^{131}I-labeled nanoparticles. The scintigraphic images show clear evidence of selective tumor localization of the ^{131}I-labeled nanoparticles in all three mice. One hour after injection, the tissue distribution of the ^{131}I-labeled nanoparticles was not distinguishable due to the background radioactivity by the nanoparticles that remained circulating in the bloodstream. Two days after injection, tumors appeared hyperintense relative to other tissues, indicating a preferential accumulation in tumor tissues. With increasing time, the scintigraphic images more clearly delineated the tumor against adjacent tissues.

Extravasation of FGC Nanoparticles from Blood Vessels to Tumors. Openings between defective endothelial cells in tumors provide a transvascular transport pathway for nanoparticles to enter tumors. To specifically examine the leakage of FGC nanoparticles from blood vessels to tumors, Hoechst dye (blue fluorescence) was intravenously injected immediately prior to sacrificing mice at 3 days after the

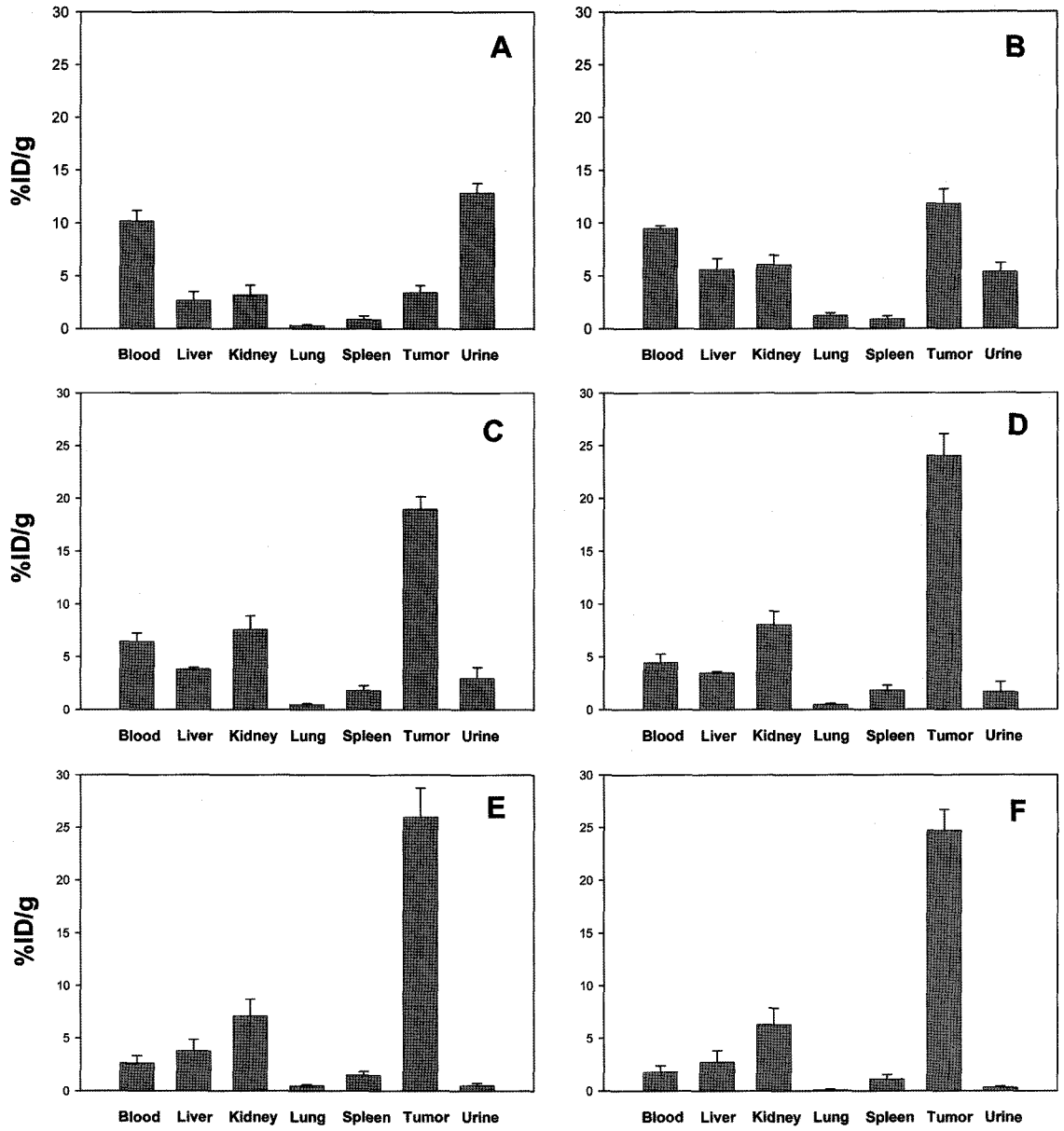

Figure 2. Tissue distribution of FGC nanoparticles 1 (A), 3 (B), 5 (C), 8 (D), 11 (E), and 14 (F) days after i.v. injection in tumor-bearing mice at a dose of 1.8 mg/kg. Each column represents the mean ± S.D. of six mice. A suspension of 1×10^6 B16F10 cells in a physiological saline was inoculated in the subcutaneous dorsa of C57BL/6J mice. On the 7th day after subcutaneous inoculation, the FGC nanoparticle suspensions (200 μL) were injected into the tail veins of the tumor-bearing mice at a dose of 1.8 mg/kg. After a definite time period, the mice were sacrificed, blood was collected, and various tissues were excised. The concentration of nanoparticles distributed in each tissue was calculated based on a standard curve which was constructed from the mixtures of predetermined amounts of nanoparticles and each tissue obtained from control tumor-bearing mice. The amount of nanoparticles in blood was also calculated based on an estimated blood volume of mice (2.18 mL/25 g).

injection of FGC nanoparticles. Figure 4 clearly shows that the hyperpermeable angiogenic tumor vasculature allows preferential extravasation of circulating FGC nanoparticles (green fluorescence). Most of the FGC nanoparticles were distributed throughout the tumors, with a higher accumulation in perivascular regions, indicating the leakage of nanoparticles via endothelial fenestration in tumors.

Discussion

The superiority of polymer-drug conjugates over low molecular weight anti-cancer compounds is mostly based on the EPR effect. In fact, the EPR effect seems to apply to all tumors. To enhance the tumor selectivity of polymeric delivery systems, we approached the EPR effect with long-

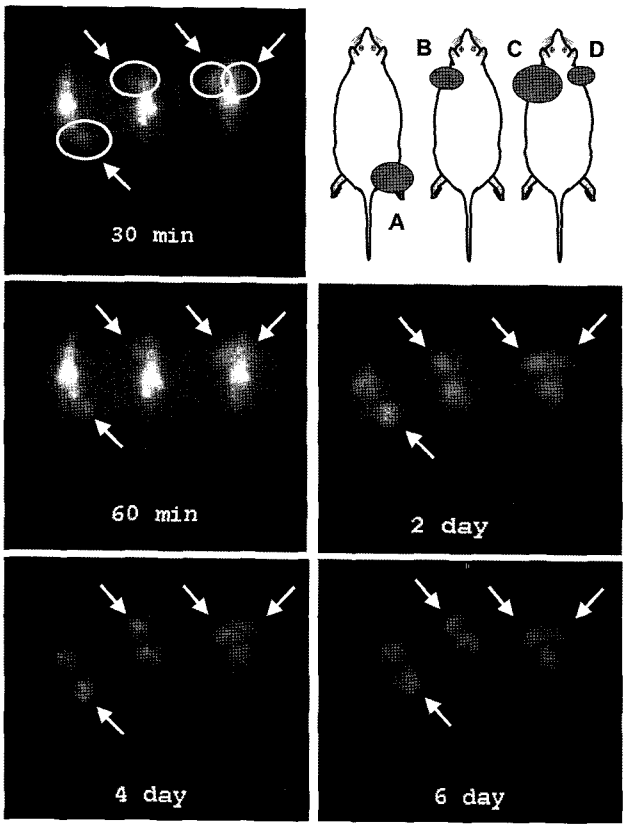

Figure 3. Gamma camera images of tumor-bearing mice 30, 60 min, 2, 4, and 6 days after i.v. administration of ^{131}I-labeled nanoparticles (mean diameter of 330 nm). A suspension of 1×10^6 SSC7 cells in physiological saline was subcutaneously injected. Two weeks after inoculation, a suspension of ^{131}I-labelled nanoparticles was injected through the tail veins of the tumor-bearing mice. Two days after injection, tumors appeared hyperintense relative to other tissues, indicating a preferential accumulation in tumor tissues. The arrows indicate the visualized tumors. Tumor volumes (mm^3) at the time of ^{131}I-labeled nanoparticle injection were A, 1900; B, 800; C, 3400; and D, 700.

circulating, self-assembled nanoparticles. We hypothesized that the delivery systems should be much larger in size than conventional polymer-drug conjugates in order to improve the selectivity to tumor tissues. After intravenous administration of either macromolecules or nano-particulate systems, their extravasations are restricted to sites where the endothelial barrier has an open fenestration, such as the liver, spleen, and bone marrow, or inflammatory tissues and tumors. In the liver, the size of open endothelial gaps can be as large as 150 nm.[27] In tumor vessels as well as certain inflammatory vessels, the size can be up to 1.2 μm.[11,17-19] Therefore, conventional polymer-drug conjugates (< 20 nm) might not actualize tumor selectivity based on the EPR effect because they are not large enough to selectively extravasate in tumors other than normal tissues with a discontinuous endothelium.

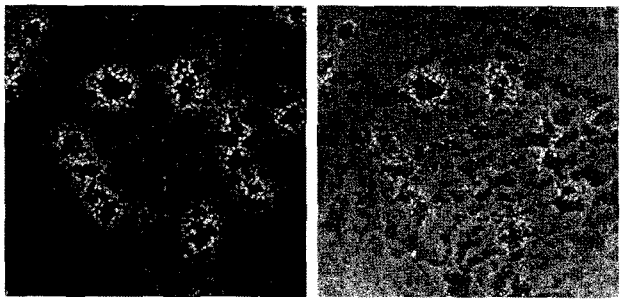

Figure 4. Visualization of extravasation of FGC nanoparticles to tumors. Tumor blood vessels were visualized by intravenous injection of Hoechst 33342 prior to sacrificing mice. Bright fluorescence (left picture) represents endothelial cells stained with Hoechst 33342. Fluorescent FGC nanoparticles (right picture) were distributed throughout the tumor, with higher accumulation in perivascular regions, indicating the preferential extravasation of nanoparticles through the hyperpermeable angiogenic tumor vasculature.

The second important hypothesis is that the delivery systems should be stable in the bloodstream, i.e., the blood circulation time of the ideal delivery systems should be long enough to exhibit tumor selectivity. Particulate systems are opsonized by plasma proteins, followed by uptake by phagocytic cells.[10,28] Liposomes and micelles, two representative colloidal particulate systems, are frequently destabilized by interaction with circulating plasma proteins, which results in dumping of drugs encapsulated in the core. When designing nanoparticles for this study, we selected chitosan as a main component of the self-assembled nanoparticles. Due to the rigidity of the polysaccharide backbone, once amphiphilic chitosan derivatives form self-assemblies they are rarely destabilized. The self-assembled nanoparticles have a unique multicore structure. The hydrophobic multicore serves as a micro-reservoir for hydrophobic drugs, and the hydrophilic shell reduces their interaction with plasma proteins and increases their half-lives in blood circulation. The hydrophobic/hydrophilic balance of the self-assembled nanoparticles was optimized to be extremely stable in blood circulation and the hydrophobic multicore was further hardened by the emulsion/solvent evaporation method to improve colloidal stability. The self-assembled nanoparticles designed on a basis of these two main hypotheses exhibited highly selective accumulation in tumor tissues.

Numerous studies have demonstrated that particulate systems such as liposomes and micelles passively accumulate in solid tumors.[11,29-31] The extent of selective accumulation in tumors, however, depends on the type of nanoparticle as well as the hyperpermeability of tumor vasculature. Among the tested nanoparticles, PEG-conjugated liposomes have attracted considerable attention. Upon injection into the circulation system, conventional liposomes tend to be rapidly destabilized or cleared, and localized in tissues, especially

the liver and spleen. Conjugation of hydrophilic PEG to liposomes resulted in decreased interaction with plasma proteins and the cells of the mononuclear phagocytic system. PEG-conjugated liposomes showed prolonged circulation in blood, a significant decrease in uptake by tissues, such as the liver and spleen, and a corresponding increased accumulation in tumors. However, the tumoral accumulation of the self-assembled nanoparticles in the present study is substantially greater than those observed previously with particulate systems including the PEG-conjugated liposomes and micelles.

We visualized the passive tumor targeting of self-assembled nanoparticles through γ-scintigraphy. Our results of γ-images showed the enhanced tumoral distribution of the nanoparticles. Even 6 days after injection, the γ-image clearly delineated the tumor against adjacent tissues. These findings confirm that the enhanced tumoral accumulation of the nanoparticles is attributed to their long residence in the bloodstream and limited distribution in other tissues.

Acknowledgments. This work was supported by the Korean Research Foundation Grant funded by the Korean Government (MOEHRD, Basic Research Promotion Fund) (KRF-2006-D00075) and grant No. RTI04-01-01 from the Regional Technology Innovation Program of the Ministry of Commerce, Industry and Energy (MOCIE).

References

(1) Y. Matsumura and H. Maeda, *Cancer Res.*, **46**, 6387 (1986).
(2) H. Maeda, *Adv. Drug Deliver. Rev.*, **6**, 181 (1991).
(3) H. Maeda, L. W. Seymour, and Y. Miyamoto, *Bioconjugate Chem.*, **3**, 351 (1992).
(4) R. Satchi-Fainaro, M. Puder, J. W. Davies, H. T. Tran, D. A. Sampson, A. K. Greene, G. Corfas, and J. Folkman, *Nature Med.*, **10**, 255 (2004).
(5) P. J. Julyan, L. W. Seymour, D. R. Ferry, S. Daryani, C. M. Boivin, J. Doran, M. David, D. Anderson, C. Christodoulou, A. M. Young, S. Hesselwood, and D. J. Kerr, *J. Control. Release*, **57**, 281 (1999).
(6) P. A. Vasey, S. B. Kaye, R. Morrison, C. Twelves, P. Wilson, R. Duncan, A. H. Thomson, L. S. Murray, T. E. Hilditch, T. Murray, S. Burtles, D. Fraier, E. Frigerio, and J. Cassidy, *Clin. Cancer Res.*, **5**, 83 (1999).
(7) C. Li, D. F. Yu, R. A. Newman, F. Cabral, L. C. Stephens, N. Hunter, L. Milas, and S. Wallace, *Cancer Res.*, **58**, 2404 (1998).
(8) H. Maeda, J. Fang, T. Inutsuka, and Y. Kitamoto, *Int. Immunopharmacol.*, **3**, 319 (2003).
(9) K. Kim, J.-H. Kim, S. Kim, H. Chung, K. Choi, I. C. Kwon, J. H. Park, Y.-S. Kim, R.-W. Park, I.-S. Kim, and S. Y. Jeong, *Macromol. Res.*, **13**, 167 (2005).
(10) G. M. Barratt, *Pharm. Sci. Technol. Today*, **3**, 163 (2000).
(11) S. M. Moghimi, A. C. Hunter, and J. C. Murray, *Pharmacol. Rev.*, **53**, 283 (2001).
(12) R. Duncan, *Nat. Rev. Drug Discov.*, **2**, 347 (2003).
(13) L. Brannon-Peppas and J. O. Blanchette, *Adv. Drug Deliver. Rev.*, **56**, 1649 (2004).
(14) J. H. Park, S. Kwon, M. Lee, H. Chung, J. H. Kim, Y. S. Kim, R. W. Park, I. S. Kim, S. B. Seo, I. C. Kwon, and S. Y. Jeong, *Biomaterials*, **27**, 119 (2006).
(15) G. Kaul and M. Amiji, *J. Drug Target.*, **12**, 585 (2004).
(16) Y. J. Son, J.-S. Jang, Y. W. Cho, H. Chung, R.-W. Park, I. C. Kwon, I.-S. Kim, J.-Y. Park, S. B. Seo, C. R. Park, and S. Y. Jeong, *J. Control. Release*, **91**, 135 (2003).
(17) F. Yuan, M. Dellian, D. Fukumura, M. Leunig, D. A. Berk, V. P. Torchilin, and R. K. Jain, *Cancer Res.*, **55**, 3752 (1995).
(18) S. K. Hobbs, W. L. Monsky, F. Yuan, W. G. Roberts, L. Griffith, V. P. Torchilin, and R. K. Jain, *Proc. Natl. Acad. Sci. USA*, **95**, 4607 (1998).
(19) H. Hashizume, P. Baluk, S. Morikawa, J. W. McLean, G. Thurston, S. Roberge, R. K. Jain, and D. M. McDonald, *Am. J. Pathol.*, **156**, 1363 (2000).
(20) W. L. Monskey, D. Fukumura, T. Gohongi, M. Ancukiewcz, H. A. Weich, V. P. Torchillin, F. Yuan, and R. K. Jain, *Cancer Res.*, **59**, 4129 (1999).
(21) D. M. McDonald and P. Baluk, *Cancer Res.*, **62**, 5381 (2002).
(22) M. Lee, Y. W. Cho, J. H. Park, H. Chung, S. Y. Jeong, K. Choi, D. H. Moon, S. Y. Kim, I.-S. Kim, and I. C. Kwon, *Colloid Polym. Sci.*, **284**, 506 (2006).
(23) Y. W. Cho, S. A. Park, T. H. Han, D. H. Son, J. S. Park, S. J. Oh, D. H. Moon, K.-J. Cho, C.-H. Ahn, Y. Byun, I.-S. Kim, I. C. Kwon, and S. Y. Kim, *Biomaterials*, **28**, 1236 (2007).
(24) K. Manotham, T. Tanaka, M. Matsumoto, T. Ohse, T. Miyata, R. Inagi, K. Kurokawa, T. Fujita, and M. Nangaku, *J. Am. Soc. Nephrol.*, **15**, 1277 (2004).
(25) L.-M. Ching, S. Zwain, and B. C. Baguley, *Br. J. Cancer*, **90**, 906 (2004).
(26) K. J. Williams, B. A. Tefler, S. Brave, J. Kendrew, L. Whittaker, I. J. Stratford, and S. R. Wedge, *Clin. Cancer Res.*, **10**, 8587 (2004).
(27) F. Braet, R. Dezanger, M. Baekeland, E. Crabbe, P. van der Smissen, and E. Wisse, *Hepatology*, **21**, 180 (1995).
(28) R. L. Juliano, *Adv. Drug Deliver. Rev.*, **2**, 31 (1988).
(29) F. Yuan, M. Leunig, S. K. Huang, D. A. Berk, D. Papahadjopoulos, and R. K. Jain, *Cancer Res.*, **54**, 3352 (1994).
(30) M. Yokoyama, T. Okano, Y. Sakurai, H. Ekimoto, C. Shibazaki, and K. Kataoka, *Cancer Res.*, **51**, 3229 (1991).
(31) N. Nishiyama, S. Okazaki, H. Cabral, M. Miyamoto, Y. Kato, Y. Sugiyama, K. Nishio, Y. Matsumura, and K. Kataoka, *Cancer Res.*, **63**, 8977 (2003).